Chapter 4
Efficient Energy Harvesting Systems for Vibration and Wireless Sensor Applications

Mustafa Doğan, Sıtkı Çağdaş İnam and Ö. Orkun Sürel

Abstract In the first part of the research, we present the design of a vibration-based energy harvesting system. Robotic flexible arm having variable cross-section is investigated to overcome serious problems, e.g. insufficient bandwidth and model inaccuracies. Most of the energy harvesting systems are linear with unimodal characteristics. On the other hand, real vibrations can be modeled as random, multi-modal and time varying systems. Hence, unimodal linear systems can give highly unsatisfactory results under certain circumstances. However, non-linear systems can have multi-modal character with increased performance in real and practical situations. In this work, tapered links are preferred with nonlinear coupling setup to provide sufficient bandwidth and output power requirements for modern applications. Thus, the proposed scheme has been proven by simulated and experimental results successfully. In the second part of the research, we present design and experimental results of an electromagnetic harvester, energy source of which is single-phase household AC power with a nominal voltage of 220 V and a frequency of 50 Hz. In this case, energy harvesting is based on the induced electromotive force (EMF) as a result of the periodic variations of the magnetic field around the AC power cord. In this part, we also discuss basic principles of a wireless sensor network design powered by electromagnetically harvested energy obtained from household alternating current.

Keywords Energy harvesting · Multi-modal vibrations · Piezoelectric · PDE modelling · Tapered beam · Flexible arm · Wireless sensors · Electro-magnetic radiation · Self-powered

M. Doğan (✉) · S.Ç. İnam · Ö. Orkun Sürel
Department of Electrical and Electronics Engineering, Baskent University, Bağlıca Kampüsü Eskişehir Yolu 20. Km Bağlıca, 06810 Ankara, Turkey
e-mail: mudogan@baskent.edu.tr

S.Ç. İnam
e-mail: inam@baskent.edu.tr

Ö. Orkun Sürel
e-mail: orkunsurel@gmail.com

N. Bizon et al. (eds.), *Energy Harvesting and Energy Efficiency*,
Lecture Notes in Energy 37, DOI 10.1007/978-3-319-49875-1_4

Nomenclature

a_1	Linear slope for tapering
$b_i(x)$	Variable height of the links due to tapering
E	Young's modulus
$I_i(x_i)$	Variable beam cross-section moment about the z-axis at the location x_i
I_{hi}	Inertia of ith hub
I_{ti}	Tip inertia of ith beam
l_i	Length of ith link
m_{hi}	Mass of ith hub
m_{ti}	Tip mass of ith beam
t	Time ($t \geq 0$)
$w_i(x_i, t)$	Flexural deflection of point i at the location x_i of ith beam
$w_{ix}(x_i, t)$	Flexural slope of point i at the location x_i where the subscript in w_{ix} denotes spatial derivative w.r.t. x
$w_{ixx}(x_i, t)$	Bending strain of point i at the location x_i
x_i	Coordinate along the axial centre of the ith beam ($0 \leq xi \leq li$)
θ_1	Angular position of the first link
θ_2	Angular position of the second link
$\rho_i(x_i)$	Variable density of the ith link depends on the cross-sectional area
τ_i	Input torque at ith motor

Abbreviation and Acronym

FEM	Finite element method
MEMS	Micro-electro-mechanical systems
ODE	Ordinary differential equations
PDE	Partial differential equations
FFT	Fast Fourier transform
EMF	Electromotive force

4.1 Introduction

Portable devices cannot be maintained steadily by limited power sources, e.g. batteries. This idea improved and motivated the research in energy harvesting area. Harvesting by vibrating resources, e.g. trains, buildings, bridges, cars, aircraft, machinery, is well-studied. One of the harvesting methods is based on piezoelectric materials that can transform electrical energy into mechanical strain or force and vice versa [1–4]. Recently, remote sensors/actuators are usually hard to reach as they are hidden in inaccessible locations such as bridges, civil buildings, even human body. Thus, energy harvesting is the only way to keep them alive [5–7].

As the first case study, e.g. [8], we consider a vibration-based harvesting system including beams with piezoelectric layers and proof mass. Most of the energy harvesting systems are linear with unimodal characteristics. On the other hand, real vibrations can be modeled as random, multi-modal and time varying systems. Hence, unimodal linear systems can give highly unsatisfactory results under certain circumstances. However, non-linear systems can have multi-modal character with increased performance in real and practical situations. In this work, tapered links are preferred with nonlinear coupling setup to provide sufficiently bandwidth and output power requirements for modern applications. Thus, the proposed scheme has been proven by simulated and experimental results successfully.

The flexible beams with piezoelectric layers can capture the environmental vibrations. The partial differential equations (PDE) are used to model such a challenging system due to nonlinear coupling for producing accurate and consistent results, compare with finite-dimensional models, e.g. ordinary differential equations (ODE) or finite element method (FEM), approaches, refer to [9, 10]. Thus, we will use the infinite-dimensional model in [9] for the energy harvesting system.

Optimal geometry of flexible links can be investigated to improve some features, e.g. low mass, low moments of inertia and high natural frequencies, e.g. see [11]. Besides, large bandwidth is required for fast and stable motion, can be achieved with high fundamental frequency, e.g. refer to [12]. Therefore, non-uniform cross-section is implemented for the links in this research.

The tapered beam structure and inherent non-linearity of the flexible arm model are indispensable to improve the bandwidth and output power. Thus, different from the literature, e.g. cantilever beams with permanent magnets, see [13–18], we do not use magnets, multiple beam-mass systems and lumped parameter models to increase the bandwidth and/or to introduce the non-linearity. One of main contributions is that the proposed structure is simple enough to catch multi-modality and nonlinearity.

As the second case study, we will deal with an energy harvesting case for wireless network sensors. Wireless sensor nodes typically have power requirements as low as microwatts, and as the batteries suitable for wireless sensor have limited lifetimes of the order of a few years, powering such systems by energy scavenging is an interesting and practical alternative since sensor nodes will no longer require the occasional battery replacement [19].

We consider a household power consumption detector for real time monitoring. Real time power consumption monitoring helps customers be more informed about their energy consumption and have greater control of their monthly costs. Our detector is based on a sensor with a current sense transformer which is powered by electromagnetically harvested energy originated from the AC source and is capable of wireless communication [20]. The detector transmits its readings wirelessly to a computer or a mobile terminal.

4.2 Vibration-Based Energy Scavenger

The power spectrum of the proposed system is significantly improved by non-uniform geometry of the links, especially for low frequency band that covers the most of practical ambient vibrations. The flexible robot arm configuration and equations of motion for the system are obtained with the extended Hamilton's principle, see extensive work in [8, 9].

4.2.1 Energy Harvester Design

Usual vibration sources have random, multi-modal and time varying characteristics. Hence, unimodal linear systems could be rather inefficient compared to non-linear systems that are capable of responding over a broad frequency range, thus performing better in realistic vibration spectrum.

The proposed novel energy harvesting system with tapered geometry of the flexible arm, covered with thin piezoelectric materials. The analytic model which is developed in [8, 9], are modified with damping terms and external excitation. Two kinds of damping mechanisms are added to the model in [9]: viscous damping and Kelvin–Voigt (or strain-rate) damping. This will be helpful for modelling due to its extreme sensitivity to mechanical damping for the power output under resonance excitation. Therefore designing the energy harvester beam to have less damping can be more important than choosing the right piezoelectric material [21]. Modified equations (PDE) of motion that includes damping terms are given in [8]. The vibration modes will be distributed over rich spectrum content due to non-linear coupling as rigorously proven in [8]. On the other hand, tapered beam geometry provides uniform strain field, e.g., trapezoidal geometry can supply efficiently more than twice the energy per unit volume than the rectangular one [22]. Besides, increasing the slope of tapering improves bandwidth [23, 24]. The proposed energy harvesting system can be easily implemented due to its simple geometry and structure.

4.2.2 Simulation Results

The proposed harvesting system is simulated using a MATLAB code. The PDEs are discretized in both spatial and time domains using finite difference method. In order to avoid complexity of the fourth-order derivative approximation, the second-order derivative approximation has been managed by using intermediate states that corresponds to physical variables such as deflections, velocity and bending moments, e.g. refer to [25]. The same method was also applied successfully and proven in [26]. The model parameters for the system, partially given in

Table 4.1 Simulation parameters of the flexible arm

Parameter	Value
Length of links	$l_1 = 0.1$ m, $l_2 = 0.024$ m
Time step	$\Delta t = 10^{-5}$ s
Spatial steps	$\Delta x_1 = l_1/100$, $\Delta x_2 = l_2/100$
Young's modulus, E	70 GPa
Density, ρ	2742 kg/m^3
Thickness of links, m	$c_1 = 0.003175$, $c_2 = 0.00238$
Maximum height for tapering at the root of the link	$b_o = 0.0654$ m
Linear slope for tapering	$a_1 = 0.12$, and 0.28
Hub inertias, kg m^2	$I_{h1} = 0.0055$, $I_{h2} = 0.0068$
Tip inertias, kg m^2	$I_{t1} = 0.0139$, $I_{t2} = 0.00024$
Hub mass, kg	$m_{h2} = 0.678$
Tip mass, kg	$m_{t1} = 0.800$, $m_{t2} = 0.0204$
Structural damping coef., S_f	2×10^5
Viscous damping coef., V_f	1.5
Attenuation factor, a_{tt}	0.5

[9], are listed in Table 4.1. A white noise of certain power amplitudes of which peak near ±2 is applied as external base excitation [8].

The simulations are summarized in Figs. 4.1 and 4.2. The tapered beam structure and inherent non-linearity of the flexible arm model are indispensable to improve the bandwidth and output power. Increasing the slope of the beam result in robust vibrations with increased amplitudes, see Fig. 4.2.

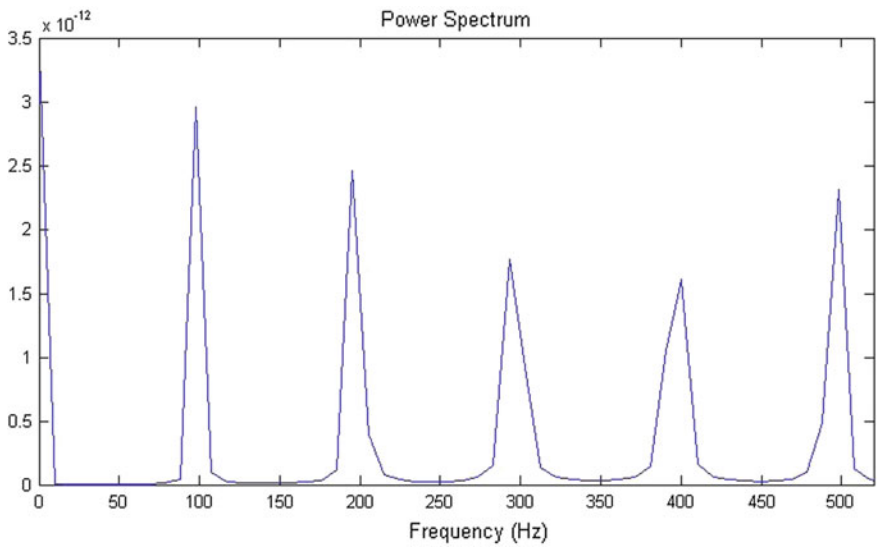

Fig. 4.1 Multi-modal character, slope = 0.12, duration = 0.1 s

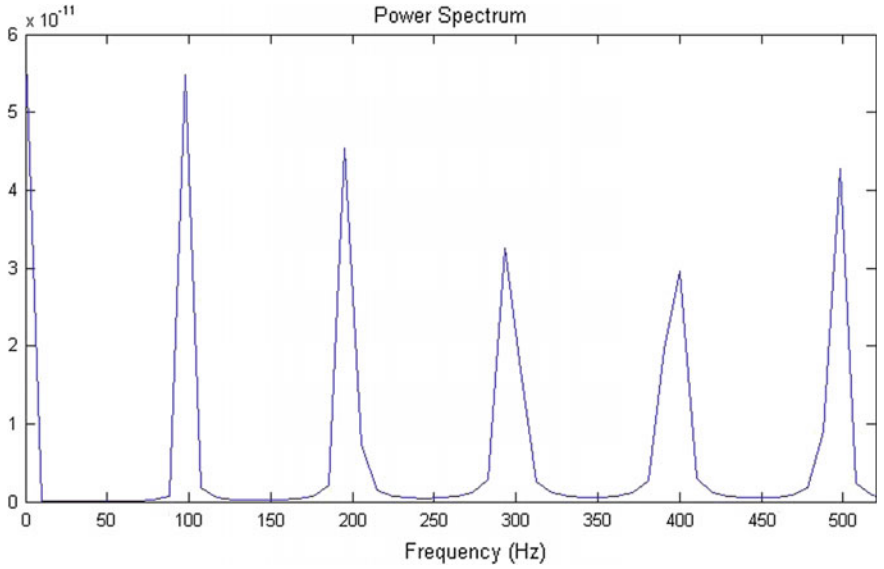

Fig. 4.2 Multi-modal character, slope = 0.28, duration = 0.1 s

Although, any kind of nonuniform cross-section can be implemented; in this particular simulation, rectangular cross-sections of given uniform thickness are examined. For small values of tip mass and tip inertia moment relative to the ones for beam, the optimum shape is approximately a linearly 'tapered' beam, see for example [12]. Consequently, the height $b_i(x)$, density, $\rho_i(x)$ and cross-section area moment $I_i(x)$ at any point can be calculated using parameters listed in Table 4.1, e.g. see [8].

4.2.3 Experimental Results

Having simple structure, stable performance and high reliability; common piezoelectric diaphragms (buzzers) are utilized as basic electronic sound components. Besides, these buzzers are also used in many sensitive equipment as shock sensors.

The main benefits of piezoelectric materials are their large power densities and ease of use. Two-link flexible arm, made of aluminum alloy, are supported by PZT buzzers. For efficient configuration, these piezoelectric materials are resided on two opposite sides of the links. The experimental setup used for measurements is shown in Fig. 4.3. Random vibration is obtained by using adjustable electronic shaker (MIKROTEK Dental Shaker RC—402) and measured by digital storage oscilloscope (RIGOL DS 5202MA, Two Channel, 200 MHz, 1 GS/s). Two-link arm are clamped to the shaker frame for robust base excitation. The second link is adjusted to freely rotate with tip mass (0.02 kg). Unamplified oscilloscope signals are

Fig. 4.3 Experiment, *1* oscilloscope, *2* data acquisition system, *3* flexible arm, *4* electronic shaker

transferred to a personal computer (PC). Built-in fast Fourier transform (FFT) utility of the digital oscilloscope are used to obtain power spectrum. All figures in this section are oscilloscope images.

Time response of the single link has expected unimodal spectrum, see Fig. 4.4 and this linear system behavior is observed for different levels of external vibrations. However, time responses of the flexible arm in Figs. 4.5, 4.6 and 4.7 are similar to that of white noise. This broadband multi-peak behavior of the harvested signal can also be observed at frequency spectrum in Figs. 4.8, 4.9, 4.10, 4.11 and 4.12 as well. The frequency value at upper right of all related figures is just an estimation of dominant frequency by oscilloscope. Change in this value throughout the all figures and also rich content of the frequency spectrum in Figs. 4.8, 4.9, 4.10, 4.11 and 4.12 show that wide bandwidth with multiple peaks have been obtained by non-linear-coupled design. Note that estimated frequency value in Fig. 4.12 is quite high as expected due to removed proof mass [8].

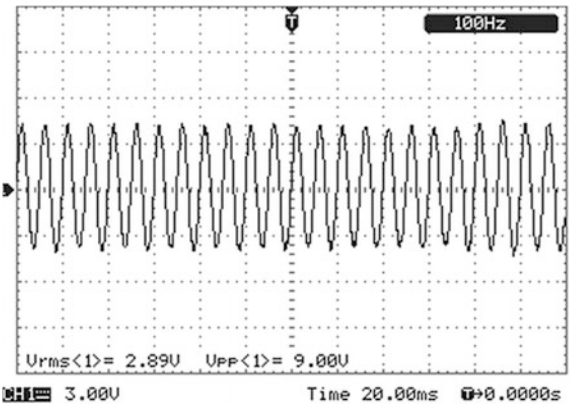

Fig. 4.4 Temporal response of the single link with tip mass

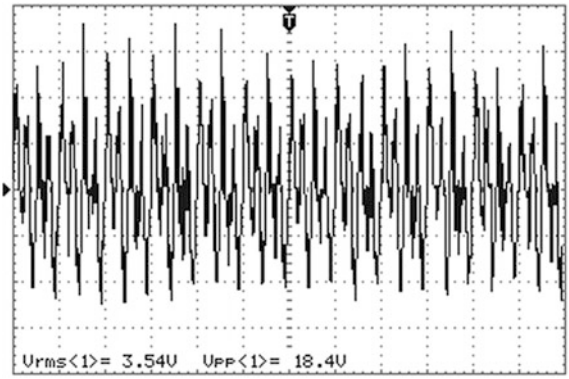

Fig. 4.5 Temporal response of the two links with tip mass with rms voltage of 3.54 V

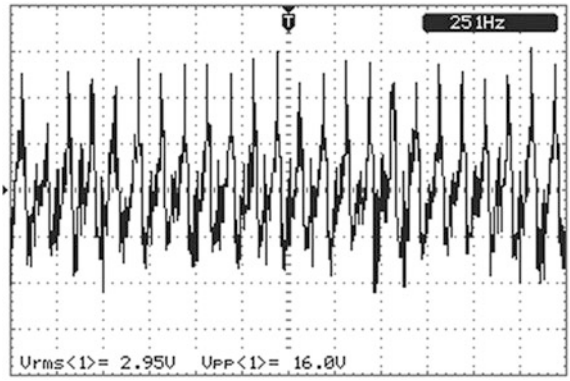

Fig. 4.6 Temporal response of the two links with tip mass with rms voltage of 2.95 V

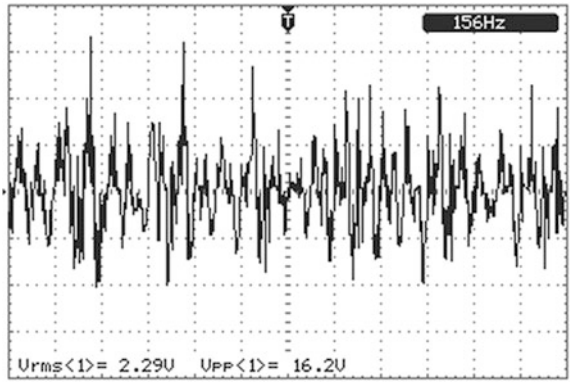

Fig. 4.7 Temporal response of the two links with tip mass with rms voltage 2.29 V

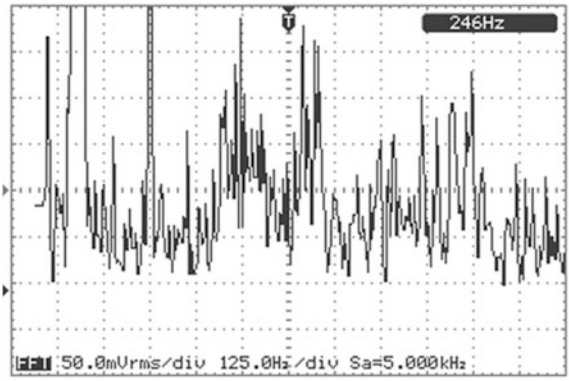

Fig. 4.8 Frequency response of the two links with tip mass with an estimated dominant frequency of 246 Hz

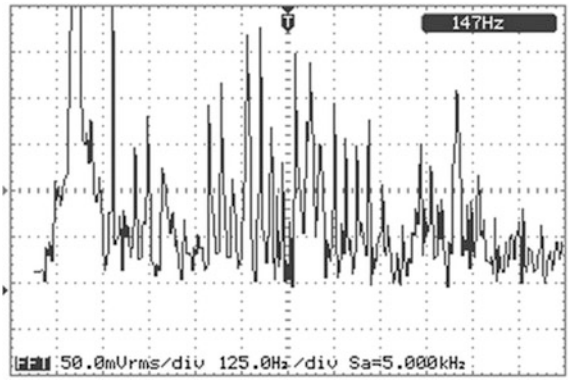

Fig. 4.9 Frequency response of the two links with tip mass with an estimated dominant frequency of 147 Hz

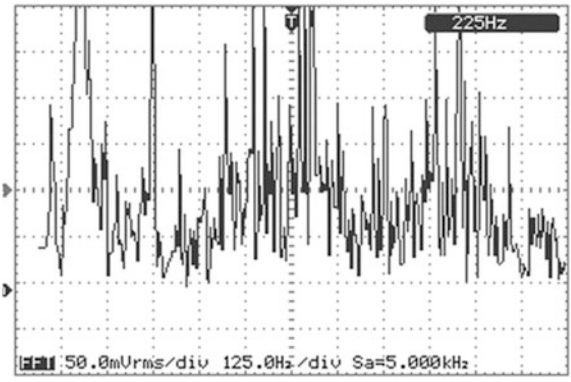

Fig. 4.10 Frequency response of the two links with tip mass with an estimated dominant frequency of 225 Hz

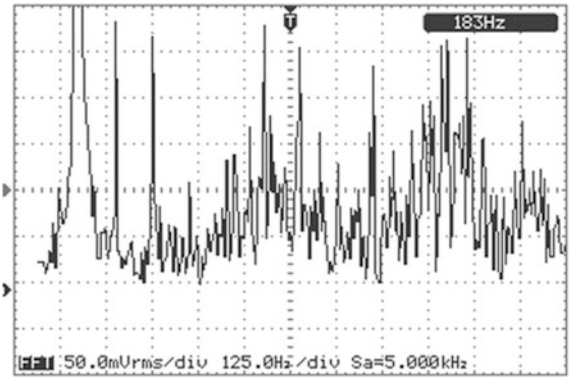

Fig. 4.11 Frequency response of the two links without tip mass with an estimated dominant frequency of183 Hz

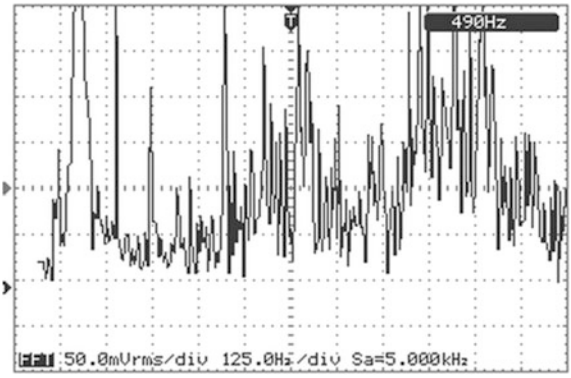

Fig. 4.12 Frequency response of the two links without tip mass with an estimated dominant frequency of 490 Hz

4.3 Wireless Sensor Network Powered by Electromagnetically Harvested Energy

In this section, we present design and the experimental results of an electromagnetic energy harvester. The source of harvested energy is single-phase household AC power with a nominal voltage of 220 V and a frequency of 50 Hz. We also discuss the use of harvested energy to power a wireless sensor network.

4.3.1 Energy Harvester Design

Energy harvesting is based on the induced electromotive force (EMF) due to change in the magnetic flux as a result of the periodic variations of the magnetic field around the AC power cord. Using Faraday's Law of Induction, it is seen that amplitude of induced EMF is proportional to four quantities: Frequency of the alternating current (AC), amplitude of the alternating current, number of turns of the

coil and the area enclosed by the coil. We are interested in harvesting power from a sub-kHz frequency and our typical current amplitude are at most of the order of a few 10 Amperes. Moreover, we have to restrict the area enclosed by the coil due to two reasons: Firstly, both magnetic field strength falls dramatically around a wire with distance. It typically changes with 1/r for very long straight wires, but in real life problems where the length of the straight part of the wire is of the order the geometric dimensions of the coil this decrease might be more substantial. Secondly, we seek for a harvesting solution that is as compact as possible. Thus, we try to increase the number of turns of the coil as much as possible without significantly extending the size of the coil. We also choose the type of the wire to ensure that it is not too thin to limit the total resistance and it is not too thick to limit the overall size of the coin.

Properties of the coil used as the energy harvester are listed in Table 4.2. Figure 4.13 shows geometry of the coil.

To harvest energy from the AC wire, we work on three different experimental setups. For the first and second setups (see top left and top right panels of Fig. 4.14), we separated the phase wire from the neutral wire so that they are more than 30 cm away. Then, as for the first setup, we place the phase wire close to the coil to enhance the magnetic flux and thus the amplitude of induced EMF. Similarly to test the amount of decrease in the harvested energy with increasing distance from the phase wire, we increase the distance between the phase wire and the coil. Thirdly, to increase the magnetic flux even further, we place both phase and neutral wires in the opposite edges of the coil (see bottom panel of Fig. 4.14). For all of these setups, the wire (or wires) are carefully held on the same plane with the area enclosing the coil.

Table 4.2 Properties of the coil used as the energy harvester

External dimensions	315 mm(L) × 75 mm(W) × 25 mm(D)
Internal dimensions	260 mm(L) × 35 mm(W) × 25 mm(D)
Number of turns	1,260 turns
Wire type	25AWG (cross-sectional area 0.45 mm^2)
Total resistance	94 Ω

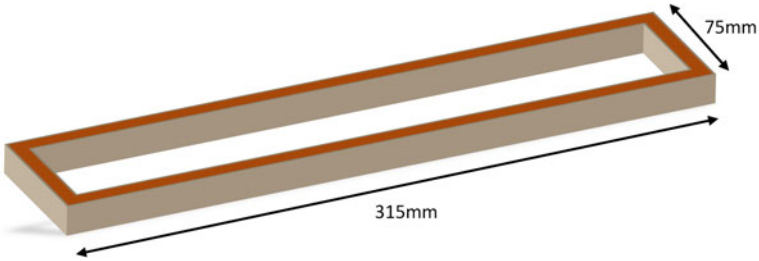

Fig. 4.13 Geometry of the coil used as the energy harvester

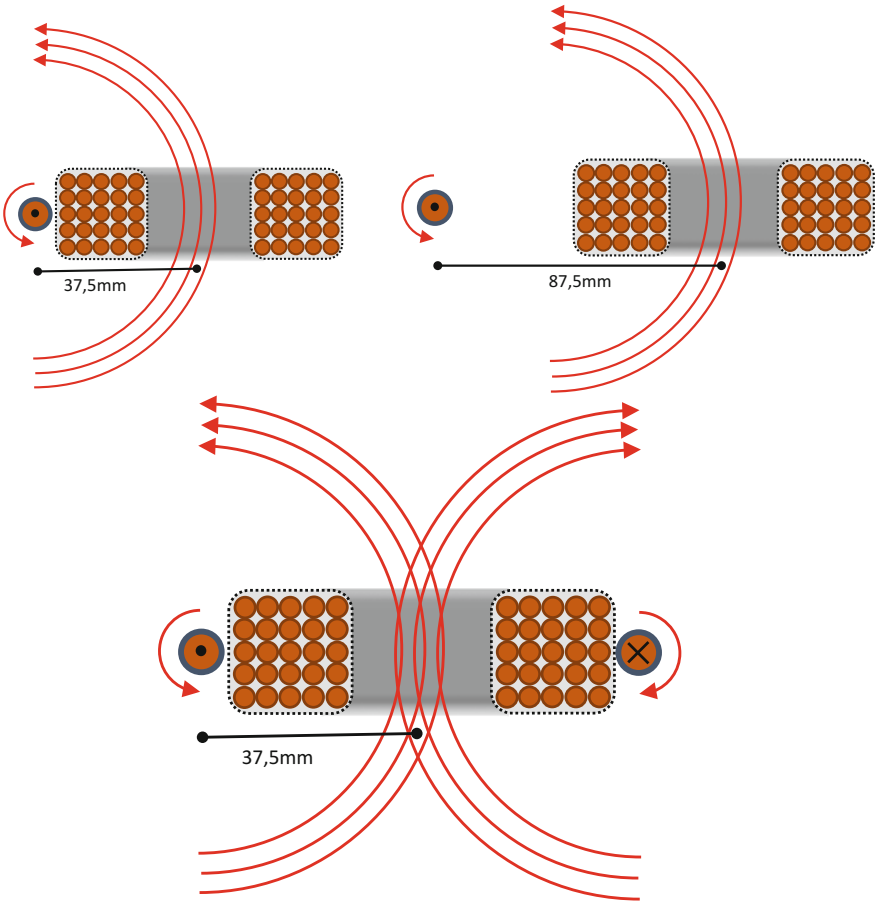

Fig. 4.14 Edge-on views of the coil corresponding to three different experimental setups. For all setups, the wires and the area enclosed by the coil lie on the same plane to maximize magnetic flux passing through the area (*red arrows* denote magnetic field line directions). *(Top left)* phase wire (separated from neutral wire) is placed close to the coil. *(Top right)* phase wire (separated from neutral wire) is placed farther away from the coil. *(Bottom)* phase and neutral wires are placed close to the coil to further enhance the magnetic flux

4.3.2 Experimental Results

In Fig. 4.15, a sample oscilloscope view obtained by measuring the voltage across the ends of the coil when it is placed close the phase wire is shown.

For the three setups shown in Fig. 4.14, we study two cases: Either AC power cord is connected to a 1000 W heater or a 2000 W heater. We measure current as a function of voltage (see left panels of Figs. 4.16, 4.17, 4.18, 4.19, 4.20 and 4.21).

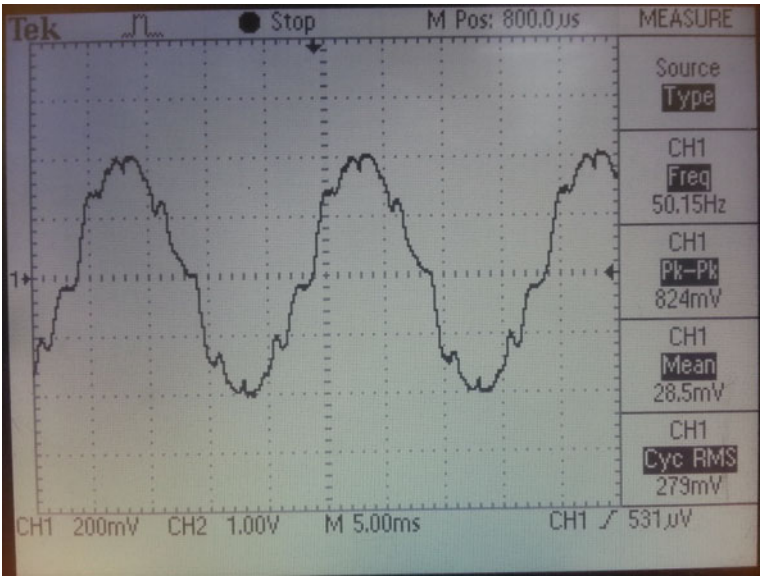

Fig. 4.15 A sample oscilloscope view obtained by measuring the voltage across the ends of the coil when it is placed close to the phase wire

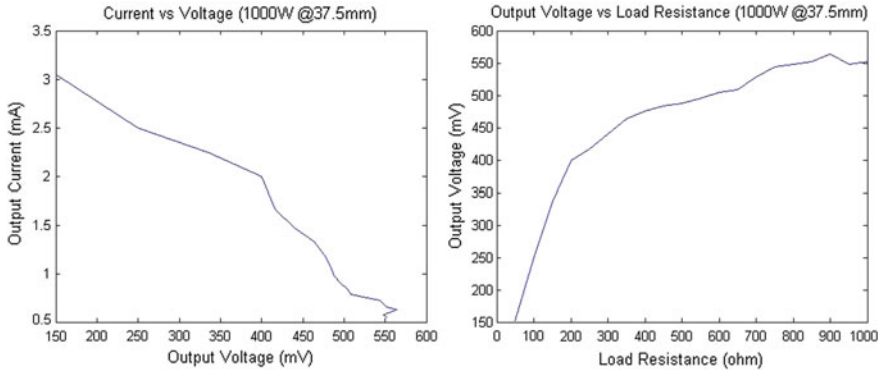

Fig. 4.16 *(Left)* current versus voltage and *(right)* output voltage versus load resistance plots for the first experimental setup and a cord connected to a 1000 W heater

We also alter the load resistance and measure corresponding voltages (see right panels of Figs. 4.16, 4.17, 4.18, 4.19, 4.20 and 4.21).

We also measure harvested and dissipated power as a function of load resistance for three experimental setups for the cases of AC power cord connected to a 1000 and a 2000 W heater (see Figs. 4.22, 4.23, 4.24, 4.25, 4.26 and 4.27).

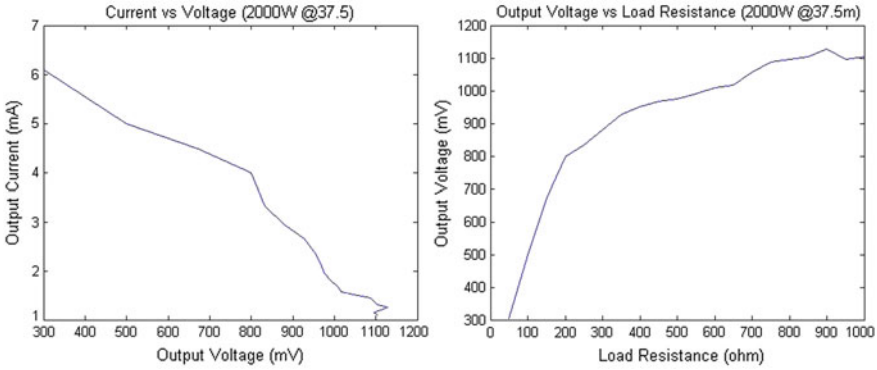

Fig. 4.17 *(Left)* current versus voltage and *(right)* output voltage versus load resistance plots for the first experimental setup and a cord connected to a 2000 W heater

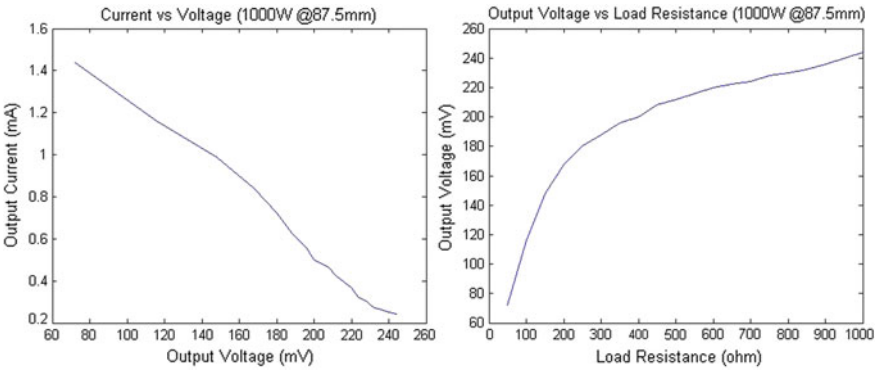

Fig. 4.18 *(Left)* current versus voltage and *(right)* output voltage versus load resistance plots for the second experimental setup and a cord connected to a 1000 W heater

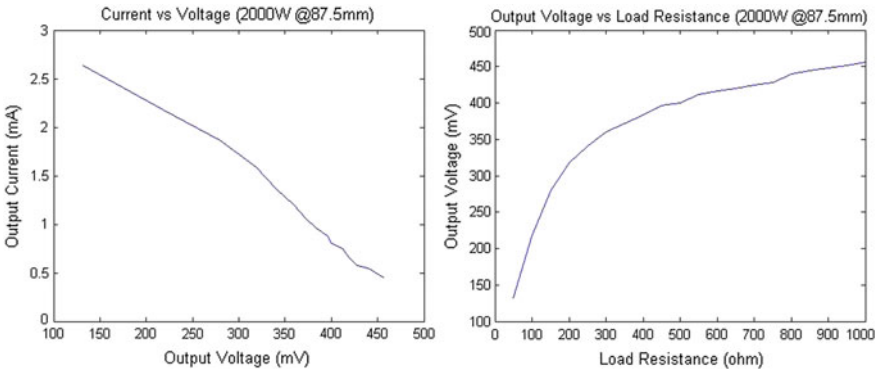

Fig. 4.19 *(Left)* current versus voltage and *(right)* output voltage versus load resistance plots for the second experimental setup and a cord connected to a 2000 W heater

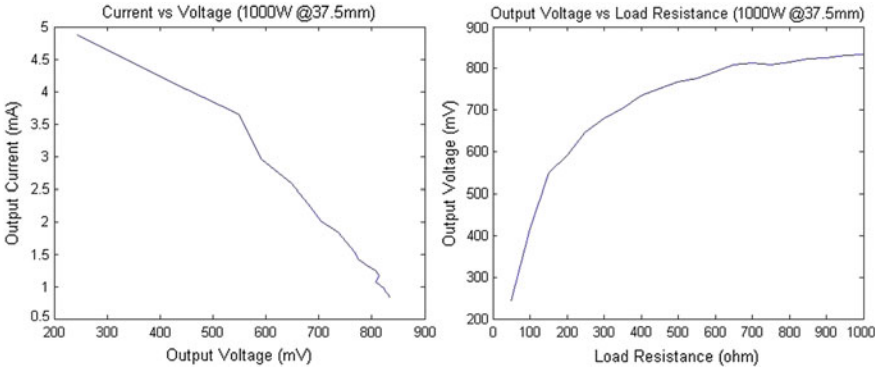

Fig. 4.20 *(Left)* current versus voltage and *(right)* output voltage versus load resistance plots for the third experimental setup and a cord connected to a 1000 W heater

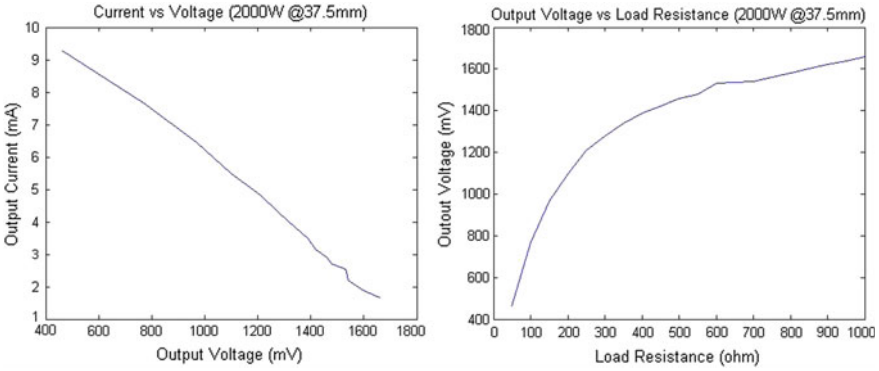

Fig. 4.21 *(Left)* current versus voltage and *(right)* output voltage versus load resistance plots for the third experimental setup and a cord connected to a 2000 W heater

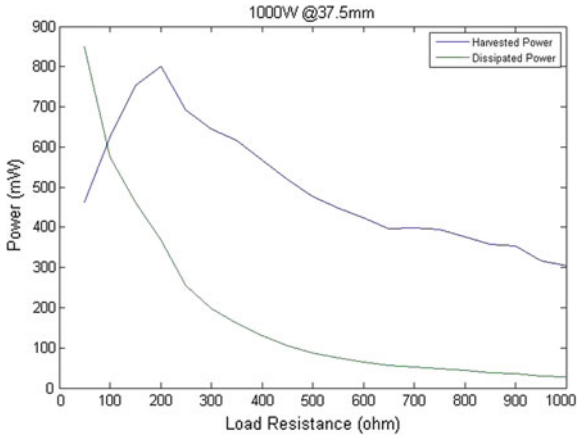

Fig. 4.22 Harvested and dissipated power as a function of load resistance plot for the first experimental setup and a cord connected to a 1000 W heater

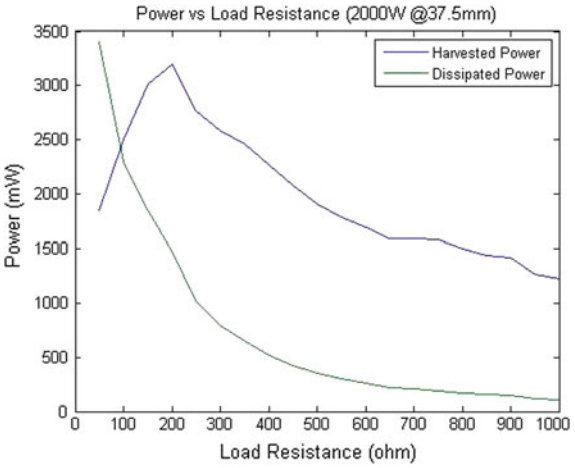

Fig. 4.23 Harvested and dissipated power as a function of load resistance plot for the first experimental setup and a cord connected to a 2000 W heater

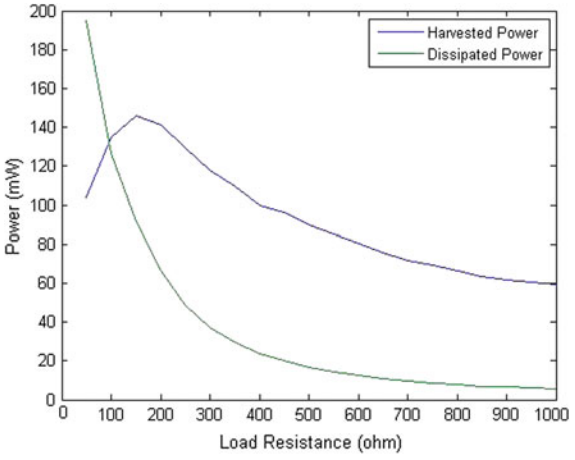

Fig. 4.24 Harvested and dissipated power as a function of load resistance plot for the second experimental setup and a cord connected to a 1000 W heater

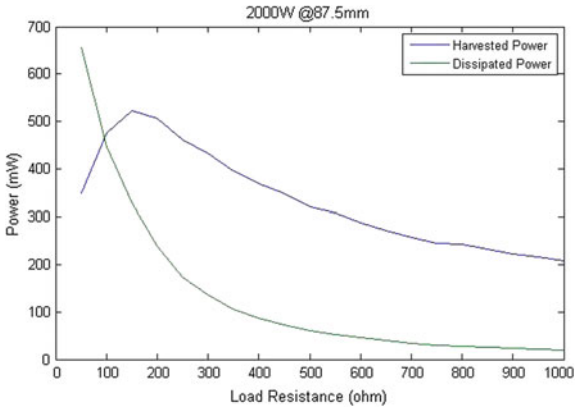

Fig. 4.25 Harvested and dissipated power as a function of load resistance plot for the second experimental setup and a cord connected to a 2000 W heater

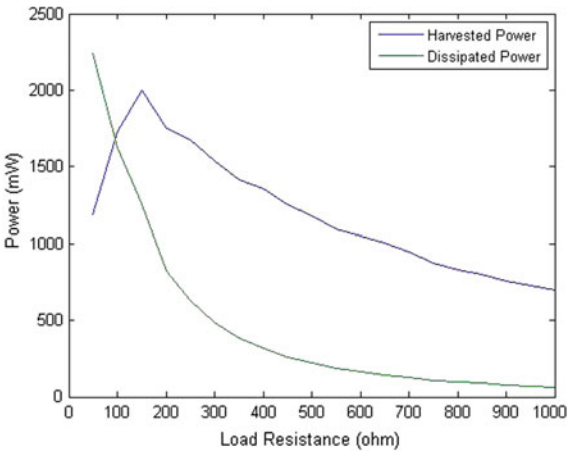

Fig. 4.26 Harvested and dissipated power as a function of load resistance plot for the third experimental setup and a cord connected to a 1000 W heater

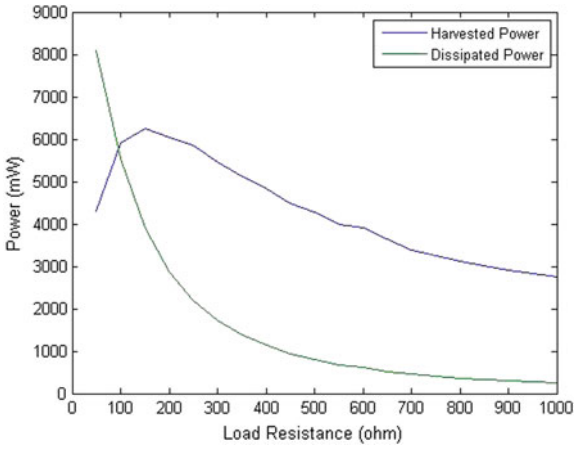

Fig. 4.27 Harvested and dissipated power as a function of load resistance plot for the third experimental setup and a cord connected to a 2000 W heater

4.3.3 Design of a Wireless Sensor Network Powered by Electromagnetically Harvested Energy Obtained from Household Alternating Current

Energy harvesting from household alternating current requires more diligent designs compared to energy harvesting from an RF field due to the fact that frequencies involved are orders of smaller compared to RF frequencies, see e.g. [27–29]. As seen from Figs. 4.16, 4.17, 4.18, 4.19, 4.20, 4.21, 4.22, 4.23, 4.24, 4.25, 4.26 and 4.27, harvested energy input from an AC power cord can be obtained very efficiently using a harvester design presented as the third experimental setup as shown in bottom panel of Fig. 4.14. For such a design, harvested powers can reach up to a few Watts for loads up to 1 kΩ in case of household currents of ≈5–10 A.

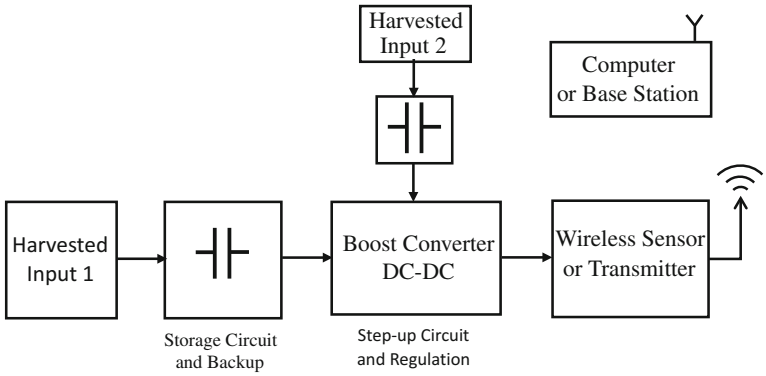

Fig. 4.28 Block diagram of a wireless sensor network powered by electromagnetically harvested energy. A single node and a computer or base station are shown only

This harvested energy can efficiently be used by a sensor network illustrated in Fig. 4.28. Such a sensor network might be used to track detailed household energy usage.

4.4 Conclusion

In this chapter, firstly we investigated the design of energy harvester by a flexible arm with non-uniform cross-section. It is proven by the simulation results that the new design method can provide efficient energy harvesting without complex structures, e.g. magnets and separated links. Coupled non-linear systems can have multi-modal character with increased performance in real and practical situations. The shape of the power spectrum is retained effectively even with some geometry and mass changes. This proves the robustness of the proposed scheme.

The tapered beam structure and inherent non-linearity of the flexible robot arm are indispensable to improve the frequency response and maximum output power. Thus, different from the literature, e.g. cantilever beams with permanent magnets, we do not use magnets, multiple beam-mass systems and lumped parameter models to increase the bandwidth and/or to introduce the non-linearity. One of main contributions is that the proposed structure is simple enough to catch multi-modality and nonlinearity.

In this work, variable cross-section links are preferred with rigorous nonlinear coupling setup to provide sufficiently bandwidth and output power requirements for modern applications. Thus, the proposed scheme has been proven by simulated and experimental results successfully.

Secondly, we design and realize an efficient energy harvester which makes use of both phase and neutral wires of a household alternating current. Having

presented our experimental results, we show that harvested powers can reach up to a few Watts for loads up to 1 kΩ for three different configurations.

We also discuss design of a wireless sensor network powered by electromagnetically harvested energy obtained from household alternating current. To power such a wireless network, it is discussed that storage/back-up and step-up/regulating circuits can be developed to feed the wireless sensors or transmitter.

References

1. Shahruz SM (2006) Limits of performance of mechanical band-pass filters used in energy scavenging. J Sound Vib 293(1–2):449–461
2. Shahruz SM (2006) Design of mechanical band-pass filters with large frequency bands for energy scavenging. Mechatronics 16(9):523–531
3. Shahruz SM (2008) Design of mechanical band-pass filters for energy scavenging: multi-degree-of-freedom models. J Vib Control 14(5):753–768
4. Shahruz SM (2008) Performance of mechanical bandpass filters used in energy scavenging in the presence of fabrication errors and coupling. J Vib Acoust 130(5):054505(9 pp). doi:10.1115/1.2950056
5. Chennault KAC, Thambi N, Sastry AM (2008) Topical review powering MEMS portable devices: a review of non-regenerative and regenerative power supply systems with special emphasis on piezoelectric energy harvesting systems. Smart Mater Struct 17(4):043001(33 pp). doi:10.1088/0964-1726/17/4/043001
6. Beeby SP, Tudor MJ, White NM (2006) Review article energy harvesting vibration sources for microsystems applications. Meas Sci Technol 17:R175–R195
7. Paradiso JA, Starner T (2005) Energy scavenging for mobile and wireless electronics. Pervasive Comput 1:18–27
8. Dogan M (2012) Efficient energy scavengers by flexible robot arm with non-uniform cross-section. IET Control Theor Appl 6(7):935–942. doi:10.1049/iet-cta.2011.0173
9. Doğan M, Morgül Ö (2010) On the control of two-link flexible Robot arm with nonuniform cross section. J Vib Control 16(5):619–646. doi:10.1177/1077546309340994
10. Luo ZH (1993) Direct strain feedback control of flexible Robot arms: new theoretical and experimental results. IEEE Trans Autom Control 38(11):1610–1622
11. Moallem M, Patel RV, Khorasani K (2000) Optimization of an actuated flexible arm for improved control properties. In: Proceedings of IEEE international conference control application, pp 709–714, Anchorage
12. Wang FY, Russell JL (1992) Optimum shape construction of flexible manipulators with tip loads. In: Proceedings of the 31st IEEE conference decision and control, Tucson, pp 311–316
13. Shahruz SM (2008) Increasing the efficiency of energy scavengers by magnets. J Comput Nonlinear Dyn 3(4):041001(12 pp). doi:10.1115/1.2960486
14. Stanton SC, McGehee CC, Mann BP (2010) Nonlinear dynamics for broadband energy harvesting: investigation of a bistable piezoelectric inertial generator. Phys D Nonlinear Phenom 239(10):640–653
15. Külah H, Najafi K (2008) Energy scavenging from low-frequency vibrations by using frequency up-conversion for wireless sensor applications. IEEE Sens J 8(3):261–268. doi:10.1109/JSEN.2008.917125
16. Sarı I, Balkan T, Külah H (2010) An electromagnetic micro power generator for low-frequency environmental vibrations based on the frequency upconversion technique. J Microelectromech Syst 19(1):14–27. doi:10.1109/JMEMS.2009.2037245

17. Ferrari M, Ferrari V, Guizzetti M, Andò B, Baglio S, Trigona C (2009) Improved energy harvesting from wideband vibrations by nonlinear piezoelectric converters. Proc Chem 1:1203–1206. doi:10.1016/j.proche.2009.07.300
18. Lin J-T, Lee B, Alphenaar B (2010) The magnetic coupling of a piezoelectric cantilever for enhanced energy harvesting efficiency. Smart Mater Struct 19:045012(7 pp). doi:10.1088/0964-1726/19/4/045012
19. Yeatman, EM (2004) Advances in power sources for wireless sensor nodes. In: Proceedings of international workshop wearable and implantable body sensor networks, pp 20–21
20. Lee V (2012) Energy harvesting for wireless sensor networks. M.S. project in Engineering—Electrical Engineering and Computer Sciences, UC, Berkeley
21. Erturk A (2009) Electromechanical modeling of piezoelectric energy harvesters. Ph D thesis, Virginia Polytechnic Institute and State University, Blacksburg, November 2009
22. Roundy S, Leland ES, Baker J et al (2005) Improving power output for vibration-based energy scavengers. Pervas Comput 1:28–36
23. Goldschmidtboeing F, Woias P (2008) Characterization of different beam shapes for piezoelectric energy harvesting. J Micromech Microeng 18(10):104013. doi:10.1088/0960-1317/18/10/104013
24. Özdemir Ö, Kaya MO (2006) Flapwise bending vibration analysis of a rotating tapered cantilever Bernoulli-Euler beam by differential transform method. J Sound Vib 289:413–420
25. Abhyankar NS, Hall EK II, Hanagud SV (1993) Chaotic vibrations of beams: numerical solution of partial differential equations. ASME J Appl Mech 60:167–174
26. Dogan M, Morgül Ö (2011) Boundary control of a rotating shear beam with observer feedback. J Vib Control 18(14):2257–2265. doi:10.1177/1077546311429145
27. Chang K-S et al (2012) Electric field energy harvesting powered wireless sensors for smart grid. J Electr Eng Technol 7(1):75–80
28. Tsunoda Y et al (2015) A small-size energy-harvesting electric power sensor for implementing existing electrical appliances into HEMS. IEEE Sens J 16(2):457–463
29. Moghe R et al (2014) A low-cost electric field energy harvester for an MV/HV asset-monitoring smart sensor. IEEE Trans Ind Appl 51(2):1828–1836